ISSN 1063-7788, Physics of Atomic Nuclei, 2020, Vol. 83, No. 10, pp. 1425–1433. © Pleiades Publishing, Ltd., 2020.

PROMISING STRUCTURAL MATERIALS

Comprehensive Analysis of Nanostructure of Oxide Dispersion Strengthened Steels as Prospective Materials for Nuclear Reactors

S. V. Rogozhkin[a,b,*], A. A. Khomich[a], A. A. Bogachev[a,b], A. A. Nikitin[a,b], A. A. Lukyanchuk[a], O. A. Raznitsyn[a], A. S. Shutov[a], A. L. Vasiliev[c,d], and M. Yu. Presniakov[c]

[a] *Alikhanov Institute for Theoretical and Experimental Physics, National Research Center Kurchatov Institute, Moscow, 117218 Russia*

[b] *National Research Nuclear University MEPhI (Moscow Engineering Physics Institute), Moscow, 115409 Russia*

[c] *National Research Center Kurchatov Institute, Moscow, 123182 Russia*

[d] *Shubnikov Institute of Crystallography, Federal Research Center Crystallography and Photonics, Russian Academy of Sciences, Moscow, 119333 Russia*

**e-mail: Sergey.Rogozhkin@itep.ru, SVRogozhkin@mephi.ru*

Received January 14, 2020; revised January 17, 2020; accepted January 17, 2020

Abstract—The enhanced mechanical properties of oxide dispersion-strengthened (ODS) steels are mainly due to the high density of homogeneously distributed oxide inclusions. It is well known that some alloying elements, such as Ti, V, and Al, play an important role in the formation of oxides/nanoclusters and influence the density and size of these inclusions. In this paper, a wide range of ODS steels containing different alloying elements were studied. The microstructural analysis was performed using transmission electron microscopy and atom probe tomography. Different types of inclusions were found in the steels: oxides of the Y–Ti–O or Y–Al–O types with sizes of ~2–15 nm, and nanoclusters (2–5 nm) enriched in Y, O, and Cr, as well as Ti, V, and Al, when these elements were present in the material. It was shown that oxides made the main contribution to the steel strengthening, while the cluster contribution was comparable with that of oxides only in Austenitic ODS and 14Cr ODS steels.

Keywords: oxide dispersion strengthened (ODS) steel, transmission electron microscopy (TEM), atom probe tomography (APT), oxide particle, nanocluster

DOI: 10.1134/S1063778820100191

INTRODUCTION

Oxide dispersion strengthened (ODS) steels have considerably higher heat resistance than conventional steels owing to a significant number of uniformly distributed oxides. Among other applications, these materials are also developed for nuclear engineering as structural materials of the first wall of future fusion reactors, materials of fuel element claddings in fast reactors, and for some structures in reactor facilities of the fourth generation [1–4]. Materials of this class are capable of withstanding temperatures up to 700°C and are expected to withstand radiation swelling up to 200 dpa [5]. The mechanical properties of ODS steels greatly depend on their nanostructure characteristics: sizes and spatial distribution of disperse inclusions (particles and oxide clusters). Note that a small amount of alloying elements (Ti, Zr, V, Al, etc.) significantly reduces the size of oxide particles and increases the density of oxides and nanoclusters in ODS steels. These structural changes provide a significant increase in the creep limit in ODS steels compared to conventional steels. Nanoscale oxide inclusions serve as dislocation pinning points and provide the capture of helium generated in transmutations under the action of reactor neutrons and radiation defects.

The quantitative analysis of oxide inclusions in ODS steels requires several complementary methods. Above all is transmission electron microscopy (TEM). The smallest inclusions and clusters can be detected with small-angle neutron scattering (SANS) [6, 7] or atom probe tomography (APT) [8, 9]. SANS allows determining the volume densities of oxides and nanoclusters. The chemical composition and spatial distribution of these clusters can be studied in detail using APT. The studies applying APT showed that the composition of nanoclusters in ODS steels differs from that of stoichiometric oxides. It was shown that ODS steels contain a high density of nanoclusters enriched in Y, O, and other alloying elements such as V and Ti (if they are present in the alloy) [8–10]. For example, the ODS Eurofer steel, which was developed on the basis of Eurofer 97 within the European Fusion Research Program [11, 12], contains both Y_2O_3 oxides

Table 1. Chemical composition of the ODS steels under study, at %

ODS	Fe	Mo	Al	Ni	Zr	Mn	Cr	W	Y	O	Ti	V	C	N	Ar	Si
Eurofer ODS	88.08	—	—	0.02	—	0.39	9.81	0.34	0.13	0.34	—	0.22	0.40	0.21	—	0.06
10Cr ODS	86.90	0.57	—	—	—	0.50	10.64	—	0.17	0.17	0.29	0.11	0.60	0.02	0.01	—
14Cr ODS	84.65	—	—	—	—	—	14.44	0.33	0.12	0.12	0.23	—	0.05	0.03	—	0.01
Austenitic ODS	67.78	—	—	14.29	—	—	15.84	0.43	0.16	0.35	0.17	0.11	0.46	0.40	—	—
KP-1	77.24	—	6.42	—	0.28	—	15.13	0.56	0.16	0.04	—	—	0.13	0.02	0.01	—
KP-3	78.29	—	6.40	—	—	—	13.82	0.55	0.16	0.37	0.18	—	0.21	—	—	—
KP-4	74.92	—	7.57	—	0.28	—	15.46	0.53	0.16	0.63	0.13	—	0.27	0.02	0.01	—

[12], and nanoclusters enriched in Y, O, V, and N [8, 9]. Note that ODS Eurofer contains about 0.2 wt % V, and this chemical element plays an important role in the cluster nucleation in ODS Eurofer. Titanium is considered the most efficient chemical element for forming nanostructures in ODS steels [13, 14]. In ODS steels containing Ti, clusters are enriched in Y, O and Ti, and their number density is higher than the density of clusters in ODS Eurofer (which does not contain Ti) [9].

At present, a wide range of ODS steels has been developed within national and/or research programs in Germany [15], France [16], Japan [4], China [17], the Republic of Korea [2], etc. The analysis of the role of strengthening inclusions in ODS steels requires a comprehensive micro- and nanostructure analysis of new ODS steels. In this paper, the nanostructure of ODS steels alloyed with different elements is investigated by the TEM and APT methods.

MATERIALS

The chemical compositions of ODS steels under study are presented in Table 1. These materials were developed at the Karlsruhe Institute of Technology (KIT, Germany), Kyoto University (Japan), Korea Atomic Energy Research Institute (KAERI, Republic of Korea), and French Alternative Energies and Atomic Energy Commission (CEA, France). All ODS steels were obtained by mechanical alloying of metal powders and Y_2O_3 powders. However, there are differences in thermomechanical treatment of these steels.

Japanese KP-1, KP-3, and KP-4 ODS steels were enclosed in a mild steel capsule and degassed in vacuum of 10^{-3} Torr at 400°C for three hours. Hot extrusion was carried out at 1150ºC to form a rod with a diameter of 25 mm, followed by annealing at 1150°C for an hour. Air-cooling was applied at the last stage.

Korean 10Cr ODS steel was first exposed to isostatic hot pressing at 1150°C for four hours at 100 MPa, which was followed by hot rolling at 1100°C, normalization at 1050°C for an hour with air cooling, and subsequent tempering at 780°C for an hour with air cooling.

German Austenitic ODS steel was exposed to isostatic hot pressing at 100 MPa at 900°C for an hour.

French 14Cr ODS steel was hot-rolled from 125 to 63 mm with subsequent reheating at 1100ºC and then hot-rolled in several stages to 2 mm.

European steel Eurofer ODS (EU-Charge) was normalized at 1100°C for 30 min with water quenching followed by air-cooled tempering at 750°C for two hours.

Eurofer ODS and 10Cr ODS steels contain 9% chromium, and Austenitic ODS and KP are high-chromium steels. Japanese KP steels also contain Al. The yttrium content is within the range of 0.12–0.17 at % in all the steels, while the oxygen content is in a rather wide range from 0.12 to 0.63 at %.

TEM STUDY OF ODS STEELS

The chemical and phase composition of ODS steels were analyzed using TEM, electron diffraction (ED), and scanning transmission electron microscopy (STEM). A Titan 80-300 S/TEM (Thermo Fisher Scientific, USA) microscope with the accelerating voltage of 300 kV, equipped with a high angle annular dark-field detector (HAADF, Fischione), was used to obtain photomicrographs in the Z-contrast mode. The qualitative and quantitative chemical analysis of specimens was performed using the energy dispersive X-ray spectroscopy (EDXS) method. The cross section specimens for STEM studies were prepared with a focused ion beam (FIB) using a Helios NanoLab 600i scanning dual-beam microscope (Thermo Fisher Scientific, USA).

The microstructure of ODS steels is shown in Fig. 1. Almost all steels consist of typical ferrite grains ranging in size from ~200 nm to 2 μm and contain oxide inclusions. 14Cr ODS steel was rolled and has elongated grains with the length of 1–6 μm and width of 50–350 nm. Austenitic ODS steel consists of austenitic grains with the sizes of 100–500 nm. An example of observed oxide inclusions is shown in Fig. 2. The size distributions of oxide inclusions are shown in Fig. 3. The quantitative analysis of observed oxides is presented in Table 2. Most of the detected inclusions are 2–10 nm in size. It is generally thought that oxide

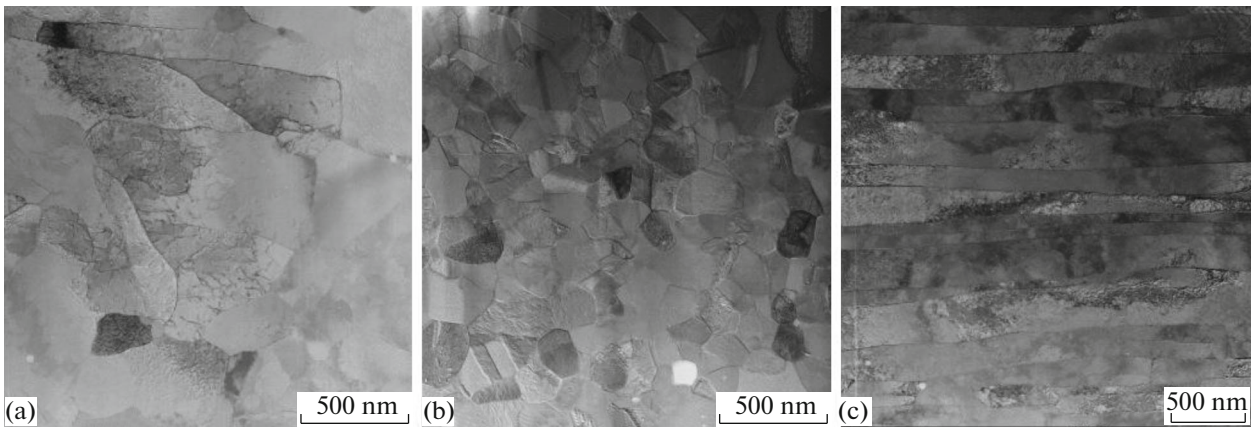

Fig. 1. Microstructure of the steels: (a) Eurofer ODS; (b) Austenitic ODS; and (c) 14Cr ODS.

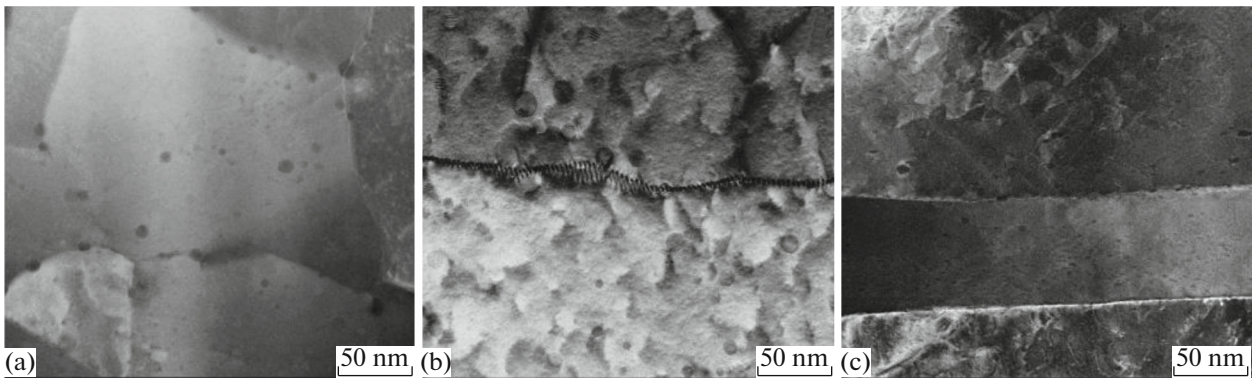

Fig. 2. Oxide inclusions in the steels: (a) Austenitic ODS; (b) KP-1 ODS; and (c) 14Cr ODS.

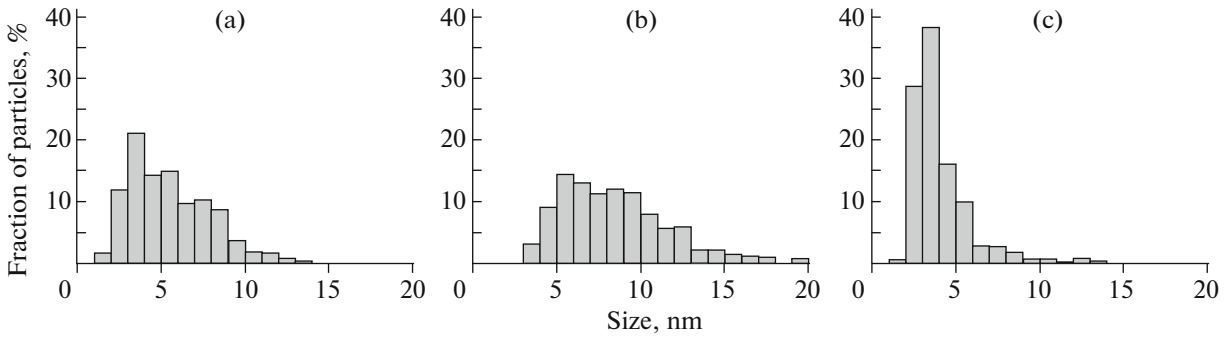

Fig. 3. Size distributions of oxide inclusions in the steels: (a) Austenitic ODS; (b) KP-1 ODS; and (c) 14Cr ODS.

inclusions of rather large sizes in Eurofer ODS steel have stoichiometry $(Y_{1.8}Mn_{0.2})O_3$ [18], while the stoichiometry of large oxides in Ti steels is $Y_2Ti_2O_7$, or Y_2TiO_5 [19]. In steels with aluminum (KP-1, KP-2, KP-3), the oxides have stoichiometry $Y_4Al_2O_9$, $YAlO_3$, $Y_3Al_5O_{12}$ [17, 20], and oxides in steels with zirconium have stoichiometry $Y_4Zr_3O_{12}$ or $Y_2Zr_2O_7$ [21, 22]. The EDX analysis showed that there were inclusions of the following types in the studied steels: Y : O, Y : Ti : O, Y : Al : O, Y : Al : Ti : O, and Al : O. An example of element mapping of oxide inclusions in Eurofer ODS steel is shown in Fig. 4. In Figs. 5–7, examples of linear profiles of element concentration in oxides of 14Cr ODS, KP-3, and Austenitic ODS steels are presented.

The highest volume density of oxide inclusions (13×10^{22} m^{-3}) was found in ODS 10Cr steel with the

Table 2. Characteristic grain sizes, mean size, and number density of oxide inclusions in the ODS steels

	Austenitic ODS	14Cr ODS	10Cr ODS	Eurofer ODS	KP-3 ODS	KP-1 ODS	KP-4 ODS
Grains, μm	0.1–0.5	Length: 1–6; width: 0.05–0.35	0.2–1.5	0.3–2	0.5–2	0.6–2	0.5–1.5
Mean size of inclusions, nm	6 ± 2	4 ± 1	3 ± 1	6 ± 2	3 ± 1	8 ± 3	5 ± 1
Volume density, m^{-3}	2×10^{22}	2×10^{22}	13×10^{22}	4×10^{22}	9×10^{22}	2×10^{22}	4×10^{22}

highest Ti content (0.29 at %) and with 0.11 at % V and 0.5 at % Mn. A slightly lower number density of oxide inclusions (9×10^{22} m^{-3}) was in KP-3 steel with 0.18 at % of Ti and 0.55 at % of W; even lower number density was found in Eurofer ODS with 0.22 at % V without Ti. The lowest number density was in KP-1 without Ti. At the same time, Austenitic ODS and 14Cr ODS had the minimum number of inclusions, although they contained 0.17 and 0.23 at % Ti. It is known that Ti is the most efficient chemical element for reducing the oxide size. At the same time, V has a significant influence in steels without Ti. We also see that some other elements may also have influence on oxide inclusions, reducing their sizes and increasing their volume density.

APT ANALYSIS OF ODS STEELS

The nanostructure of ODS steels was studied using an atom probe tomograph with femtosecond-laser assisted evaporation (APPLE-3D) developed at the Institute for Theoretical and Experimental Physics (Moscow) [23]. The data was collected at the specimen base temperature of 40–50 K in the laser evaporation mode with the wavelength of 515 nm, laser pulse duration of 300 fs, frequency of 25 kHz, and pulse energy of 0.1–1.2 μJ [24]. The pressure in the study chamber was $(5–7) \times 10^{-10}$ Torr.

The APT data reconstruction and analysis included identifying the mass spectrum and characterizing three-dimensional distributions of chemical elements in the studied volumes. In this study, the KVANTM-3D software package was used for data analysis [25]. The general Bas reconstruction method was applied to reconstruct the positions of atoms. The method provided calculating reverse projection of each ion detected using the tip radius of the specimen and the distance between the specimen and the detector [26].

The algorithm of maximum separation was used to characterize nanosize features. In this algorithm, the local environment of each atom within a small sphere with diameter d_{max} was checked. If in the sphere the number of atoms of a certain solute element exceeded

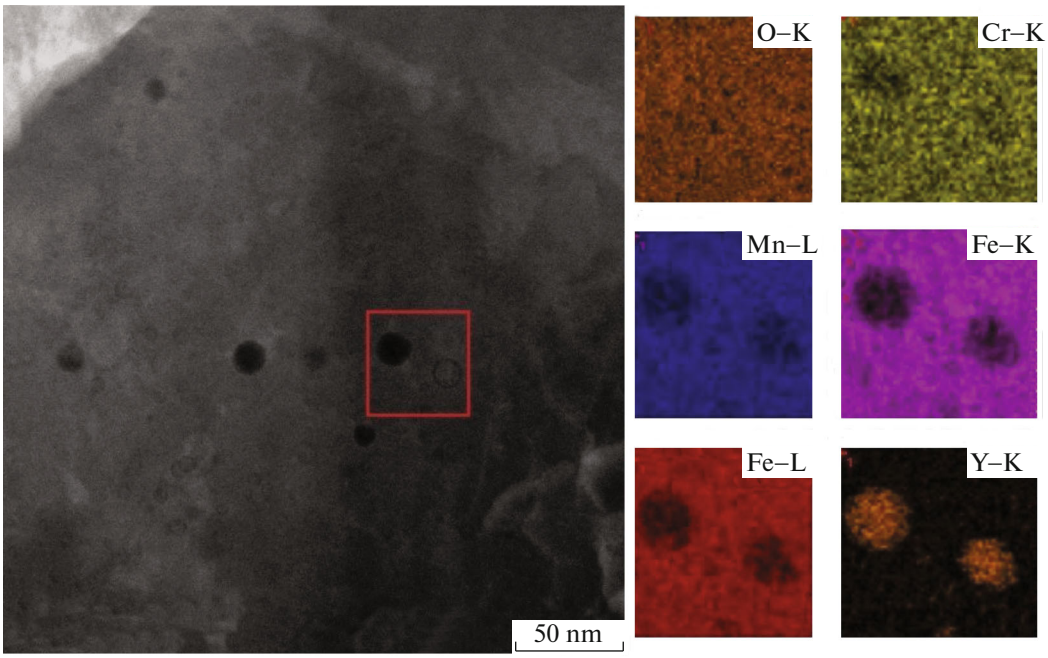

Fig. 4. Element mapping of the oxide particle in the grain of Eurofer ODS steel.

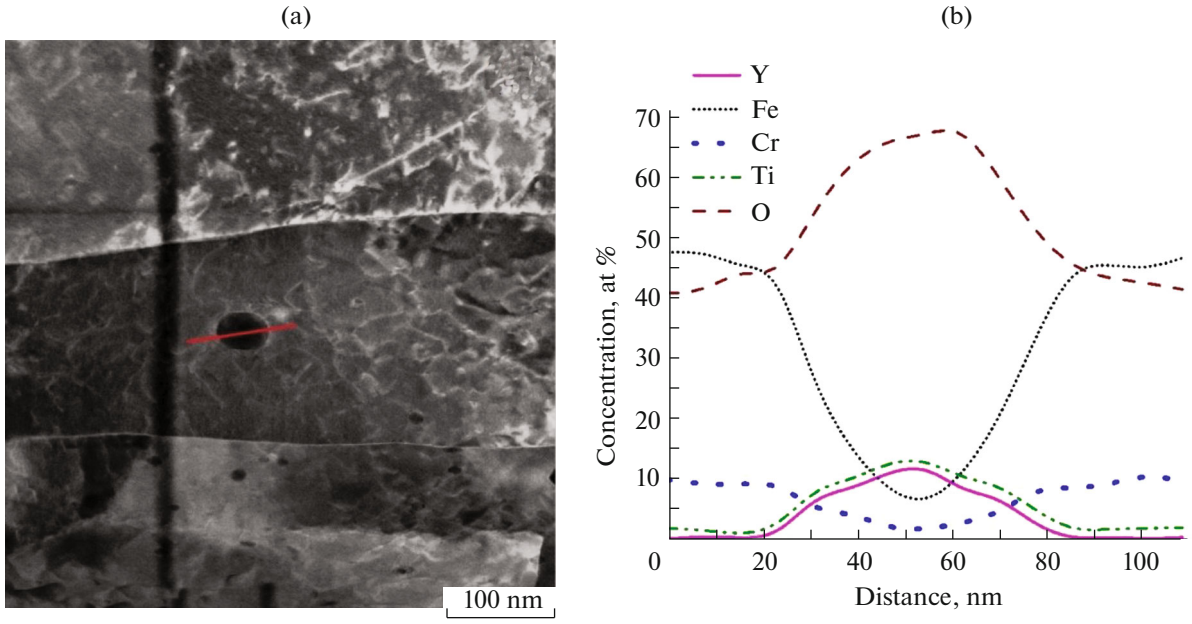

Fig. 5. (a) Image of 14Cr ODS steel obtained in the light field mode by the STEM methods. The line shows the profile that was used for microanalysis of the particle composition. (b) Linear profiles of chemical element concentrations in the oxide of 14Cr ODS steel.

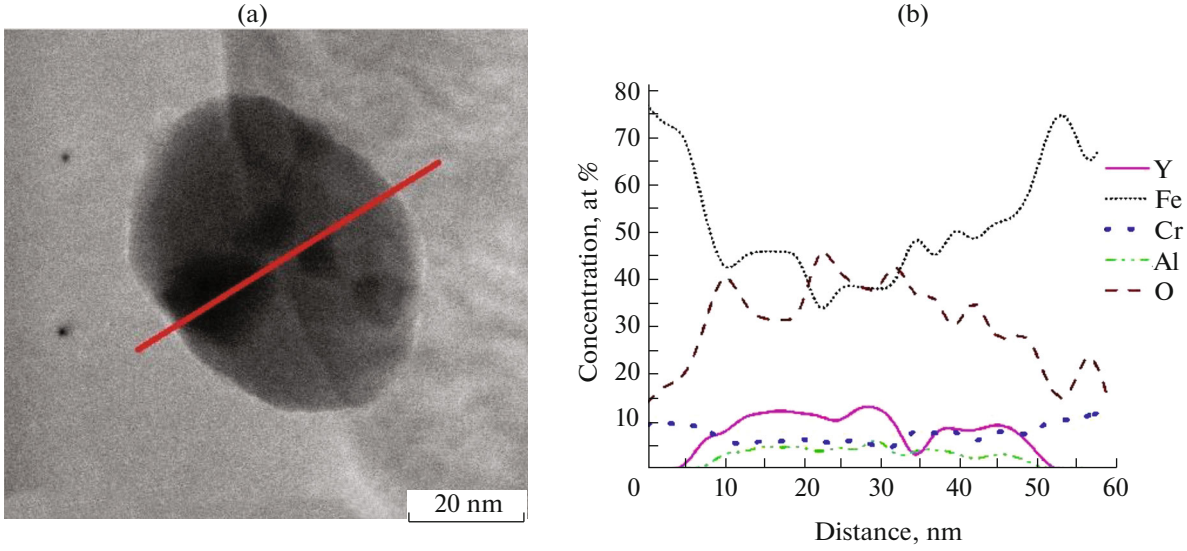

Fig. 6. (a) Image of KP-3 steel obtained in the light field mode by the STEM methods. The line shows the profile that was used for microanalysis of the particle composition. (b) Linear profiles of chemical element concentrations in the oxide of KP-3 steel.

the threshold value N_{min}, the atom at the center of the sphere was considered belonging to the cluster A. In addition, if there was another atom belonging to the cluster B next to this atom at a distance d_{max}, then these two atoms were considered to belong to the same cluster. The described procedure performed for each atom of the analyzed volume allowed identifying all possible clusters. Then an additional step was usually applied: the atoms in clusters composed of less than N_0 atoms were classified as the matrix atoms [27, 28]. If the chosen parameters were small, the effect of cluster fragmentation was observed. The choice of large parameters resulted in consolidation of closely located clusters. In this paper, the search for cluster parameters was conducted with respect to elements Y, O, Ti, V, and Zr depending on the initial steel composition and cluster enrichment in these elements. The selected search parameters for clusters d_{max} and N_{min} for the

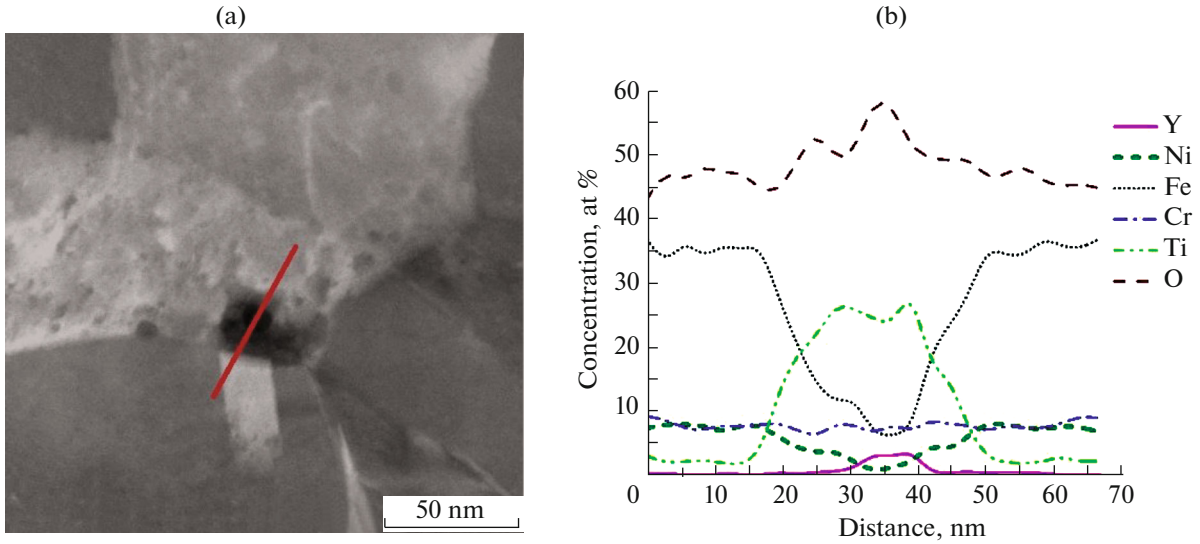

Fig. 7. (a) Image of Austenitic ODS steel obtained in the light field mode by the STEM methods. The line shows the profile that was used for microanalysis of the particle composition. (b) Linear profiles of chemical element concentrations in the oxide of Austenitic ODS steel.

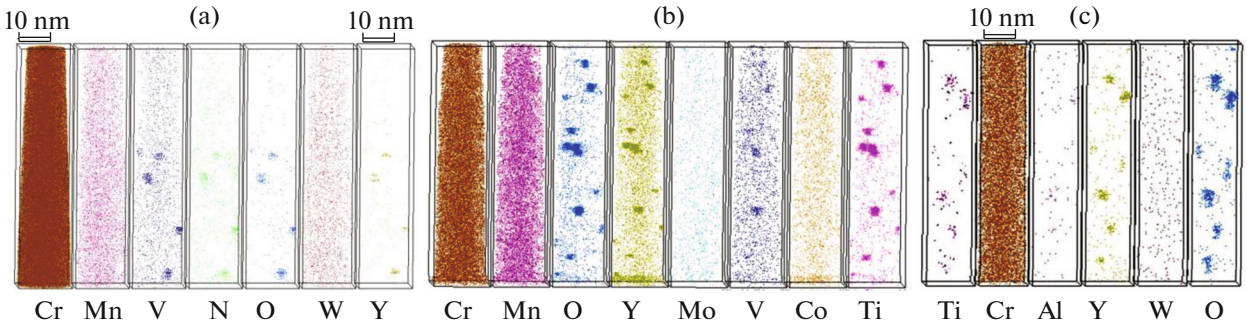

Fig. 8. Examples of atom maps of the steels: (a) Eurofer ODS; (b) 14Cr ODS; and (c) Austenitic ODS.

Austenitic ODS, 14Cr ODS, 10Cr ODS, Eurofer ODS, KP-3 ODS, KP-1 ODS, and KP-4 ODS steels were 0.7 nm and 7 atoms, 0.7 nm and 6 atoms, 0.5 nm and 6 atoms, 0.6 nm and 7 atoms, 0.7 nm and 8 atoms, 0.6 nm and 9 atoms, respectively. The minimum number of atoms in the cluster was chosen to be 50. The examples of atomic maps of three steels, Eurofer ODS, 14Cr ODS, and Austenitic ODS, are shown in Fig. 8.

The detected clusters are enriched in Y and O (see Table 3). Most of them are also enriched in Ti and Cr. Ti is absent only in the ODS Eurofer steel clusters, in whose composition it is completely absent, and in this case, V is present in the clusters. In the 10Cr ODS steel, where the V and Ti contents are close, the clusters are predominantly enriched in Ti (compared to vanadium). In steels with aluminum, the clusters are enriched in this element only in KP-3 steels, and the addition of Zr to KP-1 and KP-2 steels considerably enriches the clusters in Zr, while simultaneously depleting them in Al. The size distribution of clusters is shown in Fig. 9. The mean sizes and number density of clusters detected by APT are summarized in Table 4. Most clusters have sizes of 3–5 nm, and only in KP-1 steel are the characteristic sizes 8–10 nm. In this case, the lowest number density of clusters is detected. The highest number density of clusters ($>10^{23}$ m^{-3}) is found in Austenitic ODS and 14 Cr ODS steels.

ANALYSIS OF ODS STEEL STRENGTHENING DUE TO INCLUSIONS

The obtained data of the microscopic analysis of the structural-phase state of ODS steels make it possible to estimate the role of the found inclusions in the strengthening. The dispersed barrier hardening (DBH) model is the basic model for estimating changes in the yield strength [29]. Within this model, each barrier type contributes to the strengthening according to the Orowan formula:

Table 3. Cluster enrichment in chemical elements found by APT in ODS steels, at %

	Austenitic ODS	14Cr ODS	10Cr ODS	Eurofer ODS	KP-3	KP-1	KP-4
Cr	5 ± 2	3 ± 2	4 ± 2	10 ± 5	4 ± 2	–6 ± 3	–0.1 ± 0.2
Y	5 ± 2	1.2 ± 0.6	3 ± 2	3 ± 1	1.3 ± 0.7	10 ± 5	4 ± 2
O	11 ± 6	6 ± 3	7 ± 4	4 ± 2	4 ± 2	17 ± 8	7 ± 3
Ti	8 ± 4	4 ± 12	6 ± 3	—	6 ± 3	5 ± 3	2 ± 1
V	1.2 ± 0.6	—	0.8 ± 0.4	8 ± 4		—	—
N	—	—	—	4 ± 2		—	—
Zr	—	—	—	—		7 ± 3	2 ± 1
Al	—	—	—	—	0.8 ± 0.4	–3 ± 1	–2 ± 1

Table 4. Mean sizes and number density of clusters detected by APT in ODS steels

	Austenitic ODS	14 Cr ODS	10Cr ODS	Eurofer ODS	KP-3	KP-1	KP-4
Mean size, nm	4 ± 1	4 ± 2	4 ± 1	3 ± 1	4 ± 1	9 ± 1	4 ± 1
Number density, 10^{22} m^{-3}	28 ± 4	41 ± 5	9 ± 1	10 ± 3	13 ± 2	1.5 ± 0.6	9 ± 3

Table 5. Calculations of strengthening within the DBH model due to oxide inclusions and clusters

	Austenitic ODS	14Cr ODS	10Cr ODS	Eurofer ODS	KP-3	KP-1	KP-4
Oxides	0.44 ± 0.07	0.36 ± 0.04	0.8 ± 0.1	0.6 ± 0.1	0.7 ± 0.1	0.51 ± 0.09	0.57 ± 0.05
Clusters	0.21 ± 0.03	0.26 ± 0.06	0.12 ± 0.01	0.11 ± 0.02	0.15 ± 0.02	0.12 ± 0.01	0.06 ± 0.03
Total strengthening	0.49 ± 0.07	0.44 ± 0.07	0.8 ± 0.1	0.6 ± 0.1	0.7 ± 0.1	0.58 ± 0.06	0.57 ± 0.05

$$\Delta\sigma_i = M_T \alpha_i \mu b \sqrt{N_i d_i}, \quad (1)$$

where α_i is the barrier strength, M_T is the Taylor factor, μ is the share modulus, b is the modulus of the Burgers vector, and N_i and d_i are the number density and the mean size of this type barrier. In [30], the mean strength of the barrier of oxide inclusions was estimated as 0.59, with the maximum value of 0.80. The barrier strength for oxide inclusions obtained from in situ TEM tensile testing [31] was 0.63 at the maximum value of 0.80. In the latter experiment, the average inclusion size was 7 nm. The barrier strength of nanoclusters in 9%Cr ODS steel was estimated as 0.1–0.08 [32].

The results of calculations of strengthening due to the detected oxide inclusions and clusters within the DBH model are presented in Table 5. The strength of

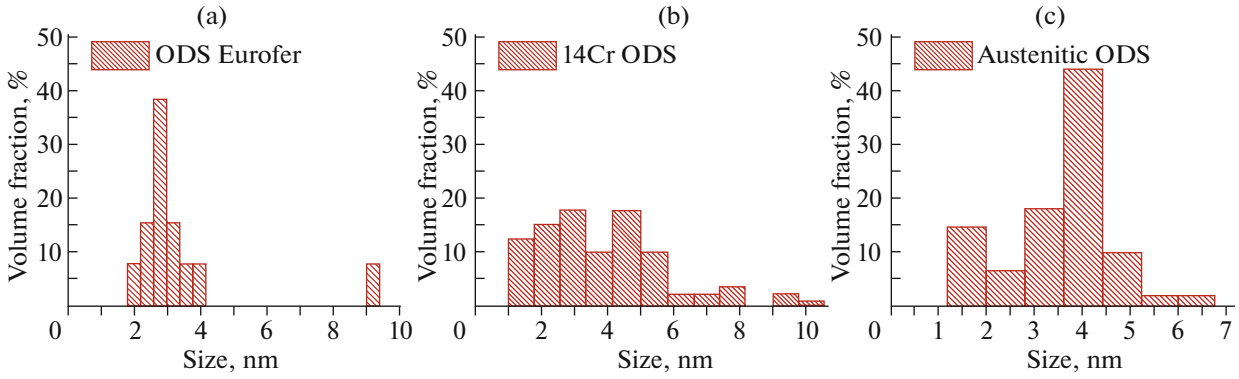

Fig. 9. Examples of size distributions of clusters in the steels: (a) Eurofer ODS; (b) 14Cr ODS; and (c) Austenitic ODS.

the barrier of oxide inclusions was chosen to be 0.63, and the strength of clusters was 0.1.

The data obtained indicate that steels with the highest number density of oxide inclusions have the highest strengthening due to nanostructure; the contribution to strengthening from nanoclusters is comparable to that of oxides only in Austenitic ODS and 14Cr ODS steels.

CONCLUSIONS

Seven ODS steels developed in Europe, Japan, and Korea were studied by the TEM and APT methods. The microscopic analysis revealed a significant number of nanoscale oxide inclusions and clusters. The mean size of the oxides varied from 3 to 8 nm, and the number density was from 2×10^{22} m^{-3} to 13×10^{22} m^{-3}. The cluster sizes were close to the oxide sizes, but their density varied from 2×10^{22} m^{-3} to 4×10^{23} m^{-3}. The calculation of strengthening of the studied ODS steels due to different types of barriers showed that oxide inclusions provided a significant contribution, and only in the case of Austenitic ODS and 14Cr ODS steels was the contribution of clusters comparable to that of oxides.

ACKNOWLEDGMENTS

We are grateful to Dr. P. Vladimirov at the Karlsruhe Institute of Technology (Germany), Professor A. Kimura at the University of Kyoto (Japan) and Dr. T.K. Kim (Republic of Korea) at the Korea Atomic Energy Research Institute for providing ODS steel specimens.

FUNDING

This work was supported by the Russian Science Foundation, project no. 17-19-01696. The equipment of the KAMIKS Shared Access Center (http://kamiks.itep.ru/) at the Alikhanov Institute for Theoretical and Experimental Physics, National Research Center Kurchatov Institute, was used for the APT analysis. The equipment of the NANOZOND Resource Center, National Research Center Kurchatov Institute (http://www.rc.nrcki.ru/pages/-main/nanozond/), was used for specimen preparation by the FIB methods and analysis by the TEM methods.

CONFLICT OF INTEREST

The authors declare that they have no conflicts of interest.

REFERENCES

1. Y. Carlan, J.-L. Bechade, P. Dubuisson, J.-L. Seran, P. Billot, A. Bougault, T. Cozzika, S. Doriot, D. Hamon, J. Henry, M. Ratti, N. Lochet, D. Nunes, P. Olier, T. Leblond, and M. H. Mathon, J. Nucl. Mater. **386–388,** 430 (2009).
2. Y. H. Jeong, W. J. Kim, D. J. Kim, J. Jang, S. H. Kang, Y.-B. Chun, and T. K. Kim, Proc. Eng. **86**, 1 (2014).
3. R. Mateus, P. A. Carvalho, D. Nunes, L. C. Alves, N. Franco, J. B. Correia, and E. Alves, Fusion Eng. Des. **86**, 2386 (2011).
4. A. Kimura, H.-S. Cho, N. Toda, R. Kasada, K. Yutani, H. Kishimoto, N. Iwata, S. Ukai, and M. Fujiwara, J. Nucl. Sci. Technol. **44**, 323 (2007).
5. J. P. Wharry, M. J. Swenson, and K. H. Yano, J. Nucl. Mater. **486**, 11 (2017).
6. R. Coppola, M. Klimiankou, R. Lindau, R. P. May, and M. Valli, Phys. B (Amsterdam, Neth.) **350**, 545 (2004).
7. Y.-S. Han, X. Mao, J. Jang, and T.-K. Kim, Appl. Phys. A **119**, 249 (2015).
8. C. A. Williams, E. A. Marquis, A. Cerezo, and G. D. W. Smith, J. Nucl. Mater. **400**, 37 (2010).
9. A. A. Aleev, N. A. Iskandarov, M. Klimenkov, R. Lindau, A. Moslang, A. A. Nikitin, S. V. Rogozhkin, P. Vladimirov, and A. G. Zaluzhnyi, J. Nucl. Mater. **409**, 65 (2011).
10. S. V. Rogozhkin, A. A. Bogachev, D. I. Kirillov, A. A. Nikitin, N. N. Orlov, A. A. Aleev, A. G. Zaluzhnyi, and M. A. Kozodaev, Phys. Met. Metallogr. **115**, 1259 (2014).
11. B. v. d. Schaaf, A.-A. F. Tavassoli, C. Fazio, E. Rigal, E. Diegele, R. Lindau, and G. Marois, Fusion Eng. Des. **69**, 197 (2003).
12. R. Lindau, A. Moslang, M. Rieth, M. Klimiankou, E. Materna-Morris, A. Alamo, A.-A. F. Tavassoli, C. Cayron, A.-M. Lancha, P. Fernandez, N. Baluc, R. Schäublin, E. Diegele, G. Filacchioni, J. W. Rensman, B. v. d. Schaaf, E. Lucon, and W. Dietz, Fusion Eng. Des. **75–79,** 989 (2005).
13. S. Ukai and M. Fujiwara, J. Nucl. Mater. **307–311,** 749 (2002).
14. S. V. Rogozhkin, N. N. Orlov, A. A. Nikitin, A. A. Aleev, A. G. Zaluzhnyi, M. A. Kozodaev, R. Lindau, A. Moslang, and P. Vladimirov, Inorg. Mater. Appl. Res. **6**, 151 (2015).
15. T. Gräning, M. Rieth, J. Hoffmann, S. Seils, P. D. Edmondson, and A. Möslang, J. Nucl. Mater. **516**, 335 (2019).
16. T. Jaumier, S. Vincent, L. Vincent, and R. Desmorat, J. Nucl. Mater. **518**, 274 (2019).
17. S. Xu, Z. Zhou, H. Jia, and Z. Yao, Steel Res. Int. **90**, 1800594 (2018).
18. M. Klimenkov, R. Lindau, and A. Möslang, J. Nucl. Mater. **386**, 553 (2009).
19. D. Bhattacharyya, P. Dickerson, G. R. Odette, S. A. Maloy, A. Misra, and M. Nastsi, Philos. Mag. **92**, 2089 (2012).
20. L. Hsiung, M. Fluss, S. Tumey, J. Kuntz, B. El-Dasher, M. Wall, B. Choi, A. Kimura, F. Willaime, and Y. Serruys, J. Nucl. Mater. **409**, 72 (2011).
21. N. H. Oono, S. Ukai, S. Hayashi, S. Ohtsuka, T. Kaito, A. Kimura, T. Torimaru, and K. Sakamoto, J. Nucl. Mater. **493**, 180 (2017).
22. P. Song, A. Kimura, K. Yabuuchi, P. Dou, H. Watanabe, J. Gao, and Y.-J. Huang, J. Nucl. Mater. **529**, 151953 (2020).

23. S. V. Rogozhkin, A. A. Aleev, A. A. Luk'yanchuk, A. S. Shutov, O. A. Raznitsyn, and S. E. Kirillov, Instrum. Exp. Tech. **60**, 428 (2017).

24. O. A. Raznitsyn, A. A. Lukyanchuk, A. S. Shutov, S. V. Rogozhkin, and A. A. Aleev, J. Anal. Chem. **72**, 1404 (2017).

25. A. A. Aleev, S. V. Rogozhkin, A. A. Lukyanchuk, A. S. Shutov, O. A. Raznitsyn, A. A. Nikitin, N. A. Iskandarov, O. A. Korchuganova, and S. E. Kirillov, State Registration Certificate of Computer Program No. 2018661876 (2018). https://www1.fips.ru/ofpstorage/Doc/IZPM/RUNWC1/000/000/002/702/112/%D0%98%D0%97-02702112-00001/document.pdf.

26. P. Bas, A. Bostel, B. Deconihout, and D. Blavette, Appl. Surf. Sci. **87**, 298 (1995).

27. M. K. Miller, *Atom Probe Tomography: Analysis at the Atomic Level* (Kluwer Academic, New York, 2000).

28. A. Cerezo and L. Davin, Surf. Interface Anal. **39**, 184 (2007).

29. G. E. Lucas, J. Nucl. Mater. **206**, 287 (1993).

30. Y. Ijiri, N. Oono, S. Ukai, S. Ohtsuka, T. Kaito, and Y. Matsukawa, Nucl. Mater. Energy **9**, 378 (2016).

31. E. Gil, N. Ordás, C. García-Rosales, and I. Iturriza, Fusion Eng. Des. **98–99,** 1973 (2015).

32. M. J. Swenson, C. K. Dolph, and J. P. Wharry, J. Nucl. Mater. **479**, 426 (2016).

Translated by N. Semenova